JOURNAL OF GEOPHYSICAL RESEARCH, VOL. 112, F04013, doi:10.1029/2007JF000760, 2007

Melt season duration and ice layer formation on the Greenland ice sheet, 2000–2004

Libo Wang,[1,2] Martin Sharp,[1] Benoit Rivard,[1] and Konrad Steffen[3]

Received 19 January 2007; revised 1 August 2007; accepted 18 September 2007; published 18 December 2007.

[1] Time series of enhanced resolution QuikSCAT images were used to map the extent and duration of surface melt and the distribution of ice layer formation on the Greenland ice sheet in the period 2000–2004. Apart from the bare ice and the mixed pixels (10%) along the ice sheet margin where melt cannot be determined reliably, annual melt duration and melt anomaly maps were produced across the ice sheet (90%) for each summer. Over the 5-year period, the mean melt duration for the ice sheet ranged from 14.3 to 20.5 d. The proportion of the ice sheet that experienced melting in a given year ranged from 44.2% to 79.2%. Extensive melt in 2002 was caused by a single melt event of a few days duration. This event was associated with the intrusion of a ridge of high pressure from the North Atlantic Ocean that brought warm air onto the ice sheet. The change in biweekly averaged backscatter between the freeze up periods in the current and previous falls was used to identify changes in the distribution of ice layers in snow between successive melt seasons. The year 2002 had the maximum melt extent and duration, and ice layer formation extended to higher elevations than in other years. Interannual changes in the distribution of ice layer formation may be associated with changes in surface height that are not necessarily indicative of mass balance changes. Mapping of ice layer formation is thus potentially useful for interpreting both real and apparent height changes measured by altimetry.

Citation: Wang, L., M. Sharp, B. Rivard, and K. Steffen (2007), Melt season duration and ice layer formation on the Greenland ice sheet, 2000–2004, *J. Geophys. Res.*, *112*, F04013, doi:10.1029/2007JF000760.

1. Introduction

[2] The Greenland ice sheet plays an important role in regional and global climate due to its high elevation and large fresh water content. The total ice-covered area on Greenland is 1.71×10^6 km^2 (including surrounding glaciers and small ice caps), and the ice volume is estimated to be 2.85×10^6 km^3, equivalent to a sea level rise of 7.2 m [*Church et al.*, 2001]. However, there are still major uncertainties in estimates of the mass balance of the ice sheet [*Cazenave and Nerem*, 2004; *Zwally et al.*, 2005]. The amount of surface melt is an important component of the mass balance, and the extent of seasonal melt on the ice sheet is a good indicator of climate change [*Bindschadler*, 1998].

[3] The extent of surface melt on the Greenland ice sheet has been studied at relatively coarse spatial resolutions (25 ~ 50 km) with both passive [e.g., *Mote and Anderson*, 1995; *Abdalati and Steffen*, 1995] and active microwave sensors [e.g., *Jezek et al.*, 1994; *Wismann*, 2000; *Nghiem et al.*, 2001]. It has also been studied at relatively fine spatial resolutions (1 ~ 6 km) with infrared sensors [e.g., *Stroeve and Steffen*, 1998; *Comiso et al.*, 2003; *Hall et al.*, 2006]. These studies reveal large interannual variations in melt extent that are related to the surface climate [*Steffen and Box*, 2001] and to changing atmospheric circulation patterns [*Mote*, 1998a, 1998b]. Using passive microwave satellite data, *Steffen et al.* [2004] demonstrated that the area of the Greenland ice sheet that experiences summer melt increased by ~16% from 1979 to 2002. More recent studies indicate that the cross polarized gradient ratio (XPGR) method used by *Steffen et al.* [2004] may underestimate the extent of melt considerably [*Ashcraft and Long*, 2006; *Tedesco*, 2007]. This raises the possibility that the change in surface melt extent may differ from that reported by *Steffen et al.* [2004].

[4] Increased melt extent is likely to be associated with a shift to higher elevations of the percolation zone of the ice sheet, where ice layers form within near surface snow and firn. This likely results in an increase in the near-surface firn density in new areas of ice layer formation that, in the absence of increased accumulation, would probably result in a decrease of surface height in these regions. The resultant elevation change would not necessarily be indicative of a shift to more negative mass balance. Thus, although airborne laser altimeters [*Krabill et al.*, 2004] and satellite radar altimeters [*Zwally et al.*, 1989, 2005; *Davis et al.*, 1998, 2000] can measure changes in ice sheet elevation,

[1]Department of Earth and Atmospheric Sciences, University of Alberta, Edmonton, Alberta, Canada.
[2]Now at Climate Research Division, Atmospheric Science and Technology Directorate, Environment Canada, Toronto, Ontario, Canada.
[3]Cooperative Institute for Research in Environmental Sciences, University of Colorado, Boulder, Colorado, USA.

0148-0227/07/2007JF000760$09.00

measurements of elevation change in the accumulation area alone are insufficient to determine whether the changes observed are due to changes in the rates of net snow accumulation or firn densification [*McConnell et al.*, 2000; *Zwally and Li*, 2002]. In the lower accumulation area of western Greenland, interannual variations of near-surface firn density alone can cause surface elevation changes of the order of ±10–20 cm [*Braithwaite et al.*, 1994]. Thus monitoring changes in the distribution of ice layer formation can help to identify areas where variable rates of firn densification may contribute to measured changes in surface height and can therefore facilitate the estimation of ice sheet mass balance from altimeter measurements.

[5] *Nghiem et al.* [2005] first attempted to detect the extent of ice layer formation in the percolation zone of the Greenland ice sheet using QuikSCAT data. Their approach was to subtract the biweekly averaged backscatter for a period before a melt season from the biweekly averaged backscatter for a period after the same melt season to determine the backscatter change. They reported extensive ice layer formation during the record melt year of 2002. However, *Nghiem et al.* [2005] used fixed dates to determine the premelt and postmelt season backscatter patterns over the whole ice sheet. This is potentially problematic because of the large spatial variation in the dates of melt onset and freeze up across the ice sheet, which means that in many areas the method does not accurately characterize the immediately preseason and postseason backscatter values. Other possible limitations of this approach for ice layer formation detection will be discussed in section 5.

[6] Although melt on Greenland has been studied extensively with microwave and infrared sensors, most previous microwave-based studies used data with relatively coarse spatial resolutions of 25 to 50 km, and recent studies indicate that the most widely used method applied to passive microwave data (XPGR) and the diurnal variation method applied to QSCAT active microwave data may underestimate the extent of melt or be inconsistent in detecting the timing and location of surface melt on the ice sheet [e.g., *Abdalati and Steffen*, 1997; *Nghiem et al.*, 2001; *Steffen et al.*, 2004; *Ashcraft and Long*, 2006; *Tedesco*, 2007]. Approaches that utilize infrared imagery detect melt through measurements of surface temperature, which can only be estimated for clear sky conditions. The surface temperature fields derived may suffer from cloud contamination [e.g., *Comiso et al.*, 2003; *Hall et al.*, 2006].

[7] In the present study, enhanced resolution QSCAT images with a spatial resolution of ~5 km [*Long and Hicks*, 2005] were used to detect surface melt on the Greenland ice sheet on a daily basis during the period 2000–2004. The Ku band QSCAT scatterometer data prove to be sensitive to surface melt and are less susceptible to detecting subsurface melt during periods of refreezing than the European Remote Sensing satellite (ERS) C band scatterometer data [*Ashcraft and Long*, 2006]. The goals of the study were to measure the extent and duration of surface melt on the ice sheet, to determine the spatial and temporal variations in melt occurrence at timescales ranging from days to years, and to investigate the major geographical and meteorological controls on the occurrence and duration of melt. In addition, we introduce a new method for the detection of interannual changes in the distribution of ice layer formation on the ice sheet and use it to identify regions of the ice sheet where interannual changes in firn characteristics and the rate of firn densification may be expected to impact the relationship between altimetry measurements of surface elevation change and surface mass balance.

[8] This paper is organized as follows: Section 2 provides a short introduction to the sensor, the enhanced resolution QSCAT products, and the in situ data used for validation. Section 3 briefly describes the snow/ice facies/zones on the Greenland ice sheet and their representation on a mean winter QSCAT backscatter image. The method used to generate a bare ice mask is described at the end of this section. Section 4 explains the method used for melt detection and presents results from its application. Section 5 presents the method used to detect changes in the distribution of ice layer formation and describes the patterns detected. Section 6 contains a summary and conclusions.

2. QSCAT Enhanced Resolution Imagery and in Situ Data

[9] The QuikSCAT satellite was launched in June 1999. It carries the SeaWinds scatterometer, which operates with a conically scanning pencil-beam antenna and makes measurements of the normalized radar cross section (σ^0) at 13.4 GHz (Ku band) frequency with two constant incidence angles: 46° at horizontal polarization over a 1400 km swath (inner beam), and 54° at vertical polarization over an 1800 km swath (outer beam). It provides 90% global backscatter coverage every 2 d with a 0.25 dB relative accuracy [*Tsai et al.*, 2000]. The resolution of the original data is about 37 × 25 km ("egg" data) and 6 × 25 km ("slice" data) [*Spencer et al.*, 2000]. Because of its wide swath and orbit geometry, QSCAT observes the polar regions multiple times each day, allowing reconstruction of surface backscatter at finer spatial resolution. Enhanced resolution products produced from QSCAT L1B data with the scatterometer image reconstruction (SIR) algorithm [*Long et al.*, 1993; *Early and Long*, 2001; *Long and Hicks*, 2005] were used in this study. The SIR algorithm was developed specifically for resolution enhancement of satellite-borne scatterometer data. It is a true reconstruction algorithm that enables resolution enhancement by utilizing multiple overlapping passes and extracting information from the side lobes of the measurement response function to generate the enhanced resolution product. Generation of the enhanced resolution product involves a trade-off between temporal and spatial resolution. Because of ascending-to-descending swath overlap and day boundary effects in the polar regions, there is large spatial variability in the timing of measurements used to construct each (ascending/descending) image [*Hicks and Long*, 2005]. The effective measurement times (local) over the Greenland ice sheet are 11:00 to 20:00 for descending pass images, and 2:00 to 5:00 for ascending pass images. Since most regions of Greenland receive 24-h daylight during the summer months and the data are available twice daily, we assume that the ice sheet surface does not change much within the period of each day represented by the enhanced resolution product. Thus we also assume that variability in the time periods covered by the enhanced QSCAT data will not introduce large errors in the derived melt onset and freeze up dates.

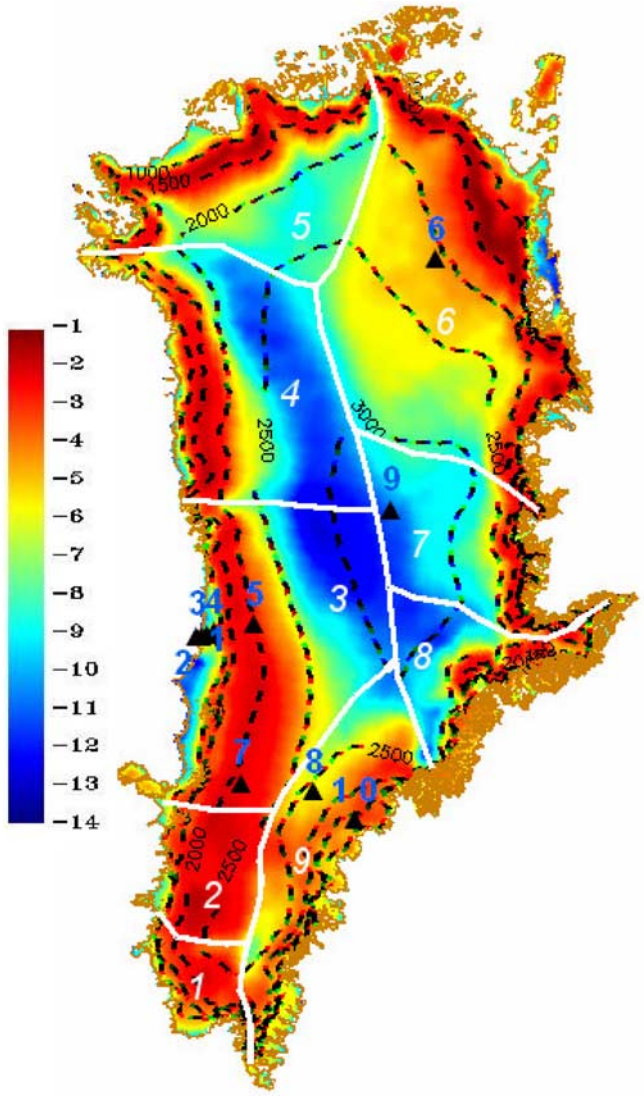

Figure 1. Average QSCAT backscatter (dB) in November 2000–2004. Dashed black contours are elevations m above sea level (asl). Black triangles and number labels indicate the locations of nine AWS and one cell in southeast (SE) Greenland: 1,2,3 indicate JAR1, JAR2, JAR3, 4 indicates ETH, 5 indicates Crawford Point1, 6 indicates Tunu-N, 7 indicates Dye-2, 8 indicates NASA-SE, 9 indicates summit, 10 indicates SE cell. White lines and number labels define the nine topographic regions.

[10] Enhanced resolution QSCAT σ^0 products are available in two forms, termed "eggs" and "slices" [*Spencer et al.*, 2000]. These differ in their spatial dimensions and shapes. Egg-based SIR images have a nominal pixel resolution of 4.45 km with an estimated effective resolution of ~8–10 km. Slice-based SIR images have a nominal pixel resolution of 2.225 km with an estimated effective resolution of ~5 km [*Long and Hicks*, 2005]. Although lower resolution, the egg products contain less noise and are less sensitive to calibration errors. The backscatter of snow as measured by QSCAT is stronger at horizontal polarization than that at vertical polarization due to the lower incidence angle at horizontal polarization [*Ulaby and Stiles*, 1981]. To capture the maximum melt signature, egg-based descending pass horizontal polarization images were therefore used to detect melt and changes in ice layer formation in this study.

[11] Near surface air temperature records from 9 automatic weather stations (AWS) (see locations in Figure 1) in the Greenland Climate Network [*Steffen and Box*, 2001] were used to assist in the interpretation of the QSCAT σ^0 data and to develop algorithms to detect melt and ice layer formation on the ice sheet. Shape files of the Greenland ice sheet taken from the Circum-Arctic map of permafrost and ground ice conditions data set [*Brown et al.*, 1998] were used as an ice mask. Only pixels fully contained within the ice sheet were used in this study so as to minimize mixed-pixel influences on the measured backscatter.

3. Surface Facies or Zones on the Greenland Ice Sheet

[12] The Greenland ice sheet can be divided into four zones based on the unique physical properties of near surface snow, firn, and ice facies [*Benson*, 1962; *Fahnestock et al.*, 1993]. The distribution of these zones is closely related to the spatial patterns of surface melt and snow accumulation and can sometimes be mapped by airborne or satellite-borne microwave or visible and near-infrared sensors [e.g., *Williams et al.*, 1991; *Fahnestock et al.*, 1993; *Jezek et al.*, 1994; *Long and Drinkwater*, 1994, 1999]. Variations in surface characteristics are clearly apparent in early winter QSCAT images. Figure 1 shows the average November backscatter for the 2000–2004 period. The high interior of Greenland exhibits very low backscatter (yellow to blue). Little or no melt occurs there during the summer (dry snow zone) and the snow therefore has a low density and relatively small grain size. The fine grains produce little volume scattering at the Ku band frequency. However, σ^0 is much lower in the southwest interior (blue areas) than in the northeast interior (yellow to light blue areas) of Greenland. This is related to the accumulation patterns over the ice sheet. The northeast is located in the precipitation shadow of the main ice sheet topographic barrier and receives minimum snow accumulation [*Ohmura and Reeh*, 1991; *Bales et al.*, 2001]. Thus the snow grains are larger in the northeast than in the southwest because they are exposed for longer at the surface. In addition, model simulations suggest that the small-scale surface roughness associated with wind scouring of the previous summer surface or wind slab may become a significant influence on backscatter where there is relatively low accumulation [*Long and Drinkwater*, 1994]. Coarser grains, a rougher surface, and a relatively larger contribution from the previous summer surface or wind slab that is not deeply buried are the most likely causes of the higher backscatter in the northeast.

[13] At lower elevations outside the interior dry snow zone, there is a region with maximum backscatter (red). This is the percolation zone, where some surface melt occurs and meltwater percolates into the snowpack and refreezes, producing ice lenses and pipes that cause the strongest backscattering of the Ku band signal. Below this region is a narrow zone of intermediate backscatter, the saturation zone (roughly the yellow band around the lower

limits of the percolation zone). Here the entire snowpack reaches the melting point in summer as a result of latent heat release by refreezing of meltwater. The firn in the saturation zone is usually denser than in the percolation zone because enhanced compaction occurs under higher temperatures [*Benson*, 1962], and a solid ice layer can be formed within the surface firn in some years. Although ice lenses can still be present in this zone, they are probably less effective backscatterers because of reduced penetration of the microwave energy into the higher density firn or ice. Since the saturation zone is so narrow, it is not easily distinguished from the percolation zone with the 4.45 km pixel spacing in the QSCAT images.

[14] At the lowest elevations, all the annual snow accumulation is melted in the summer, exposing glacier ice. In this zone, surface backscatter dominates and surface roughness determines the magnitude of the backscatter. In the early winter image (Figure 1), this region exhibits relatively low backscatter (green to blue margins) compared to the firn at higher elevations. This is probably the result of low surface backscattering from the relatively smooth surface in the bare ice zone and more volume scattering in the saturation/percolation zones.

[15] The locations of the boundaries between the surface zones vary from year-to-year depending on the extent of surface melt during the summer. Although it is possible to map the annual distribution of the zones using QSCAT data, this is beyond the scope of this study. Because of difficulties in detecting melt onset/freeze up in the bare ice zone of the ice sheet (discussed in section 4), a bare ice mask that defines the inferred maximum extent of bare ice during the 2000–2004 period was generated as follows. First, the mean November backscatter was mapped for each year. Then the minimum mean November backscatter recorded in each grid cell over the 5-year (a) period was used to outline the bare ice region. The strong gradient between low values of σ^0 in the bare ice zone and high values of σ^0 in the saturation/percolation zone was used as an indicator, and a backscatter threshold of -6.9 dB was chosen to define the upper limit of the bare ice zone. Only those low backscatter regions at elevations below 1800 m were considered to lie in the bare ice zone. A total of 78708 cells (1.58×10^6 km^2 in area) were retained for analysis after removing the bare ice and the mixed pixels along the ice sheet margin. When the bare ice and mixed pixels are included, the total ice-covered area on Greenland is 1.73×10^6 km^2 (excluding small ice caps not connected to the ice sheet). Thus the bare ice and the mixed pixels cover approximately 10% of the ice sheet area. These pixels probably all experienced melt in each summer due to their low elevations. Since we cannot detect melt in them confidently, we excluded this 10% of the ice sheet area from the analysis in this study. Thus the results presented throughout this paper are only for the 90% of the ice sheet where melt can be detected reliably. However, assuming that all of the bare ice and mixed pixels experienced melt each year, the extent of melt for the whole ice sheet was also given where relevant.

[16] Of the 9 AWS stations used in the study (Figure 1), three (JAR1, JAR2, and JAR3) are located in the bare ice zone, one (Swiss Camp (ETH)) is located in the saturation/percolation zone near the mean ice sheet equilibrium line altitude (ELA), and another (Summit) is at the ice sheet summit in the dry snow zone. The other four stations are located in the percolation zone [*Steffen and Box*, 2001].

4. Melt Detection and Results

4.1. QSCAT Melt Signature

[17] The basis for melt mapping is the reduction in Ku band σ^0 that occurs during the melt season. Liquid water in snow dramatically increases microwave absorption and masks out subsurface scattering, resulting in decreased σ^0 at the onset of snowmelt [*Ulaby and Stiles*, 1981]. Figure 2 shows 4-a time series of σ^0 and mean air temperature for the 11:00 $\sim$ 20:00 time window at the Crawford Point1 (CP1, Figure 2a), Swiss Camp (ETH, Figure 2b), and JAR2 (Figure 2c) stations on the western flank of the Greenland ice sheet (see locations in Figure 1). CP1 is located in the percolation zone at 2022 m above sea level (asl), ETH is located at 1150 m asl, near the mean ice sheet ELA, and JAR2 is located at 568 m asl in the ablation area (bare ice zone) [*Steffen and Box*, 2001]. JAR2 is close to the ice sheet margin, but still within the ice sheet mask. σ^0 decreases dramatically as the air temperature approaches the melting point at the beginning of each melt season. As the melt season progresses, however, σ^0 exhibits very different patterns of variation at the three stations. At CP1 and ETH, the period of decreased σ^0 is closely associated with the occurrence of positive air temperatures throughout the melt season; intermittent periods with air temperatures below the freezing point correspond to periods when σ^0 returns all or partway to its winter value. At JAR2, however, σ^0 increases again within a few days of melt onset, even though air temperatures remain positive. Above the ELA (CP1 and ETH), the winter snow accumulation is not completely removed during the summer, and the wet snowpack greatly reduces σ^0. Below the ELA (JAR2), however, all the winter snow is melted during the summer, exposing bare glacier ice that, even when melting, may have a rough surface with higher σ^0 than the wet snow. The timing of the increase of σ^0 depends on the snow accumulation in the previous winter and the melt rate of the snow. As a result, freeze up dates and melt season duration cannot be determined reliably for the bare ice zone. Grid cells in the bare ice zone were therefore removed from the following analysis by applying the bare ice mask described in section 3.

4.2. Melt Detection

[18] *Wang et al.* [2005] used enhanced resolution slice-based QSCAT images to detect melt on ice caps in the Queen Elizabeth Islands (QEI), Canadian high Arctic. In this region, the mean values of the winter σ^0 (W_{mn}: mean backscatter for December, January and February) increased with elevation, while the standard deviation of winter σ^0 decreased from the ice margin to the summit areas of the ice caps. These features were used to establish the σ^0 thresholds used to detect melt over the QEI. Similar behavior was found on the Greenland ice sheet, except that the highest values of W_{mn} were found in the percolation zone, rather than at the highest elevation regions of the ice sheet. This is because the dry snow zone is extensive on the Greenland ice sheet but very limited in most years on the QEI ice caps. In the percolation zone of the Greenland ice sheet, σ^0 can decrease noticeably over the winter at a single location,

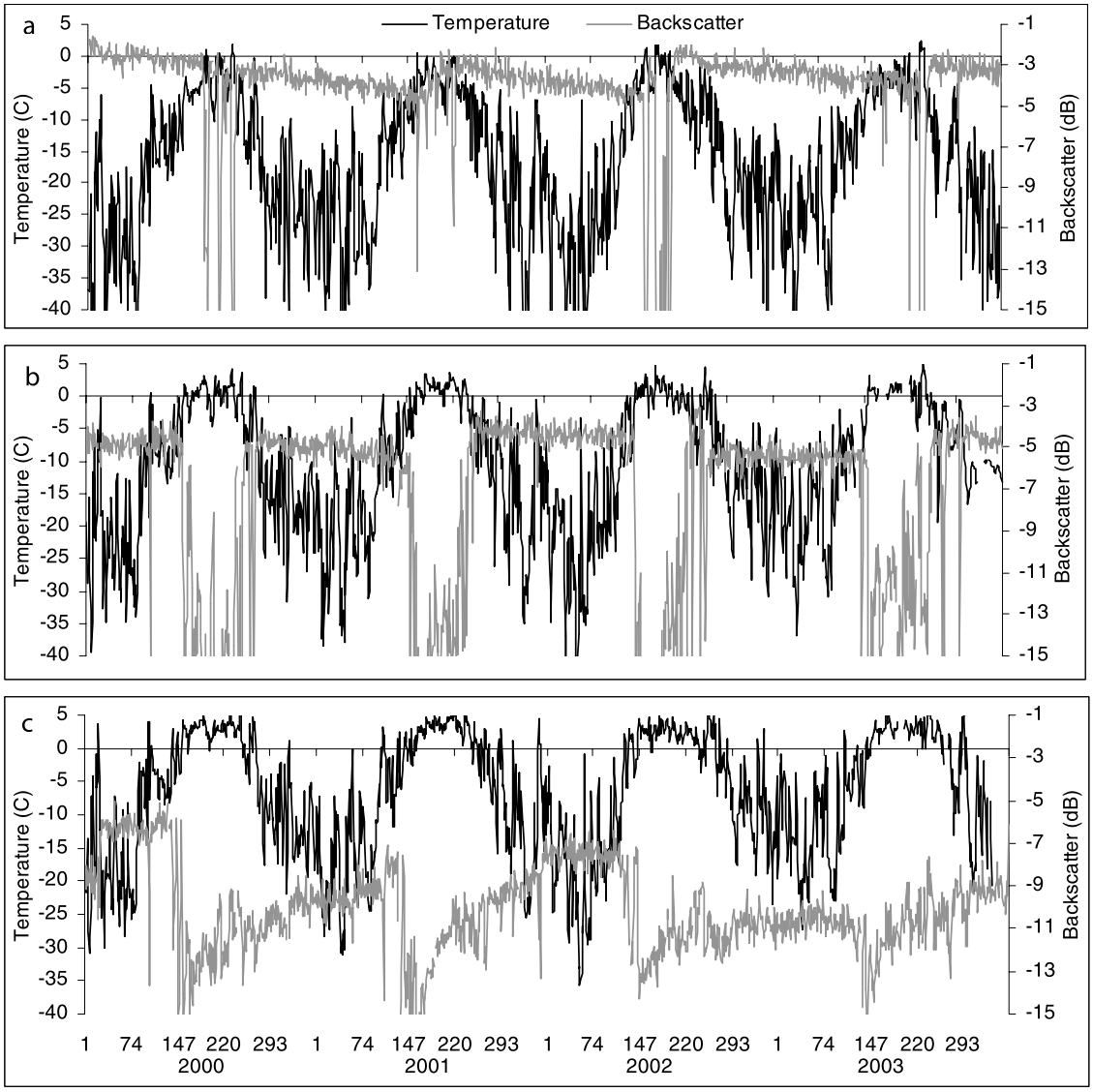

Figure 2. Time series of QSCAT σ^0 and air temperature (°C) (11:00 ∼ 20:00) at the (a) Crawford Point1 (CP1), (b) Swiss Camp (ETH), and (c) JAR2 stations on the western flank of the Greenland ice sheet (see locations in Figure 1) during 2000–2003.

(e.g., Figure 2a), while σ^0 changes relatively little over the winter on the QEI ice caps [*Wang et al.*, 2005, Figure 1]. This is because high rates of snow accumulation occur in some regions of the Greenland ice sheet [*Ohmura and Reeh*, 1991; *Bales et al.*, 2001], and the backscatter from ice lenses and pipes in the snowpack decreases as new snow accumulates on the surface [*Nghiem et al.*, 2005]. On the QEI ice caps, winter snow accumulation rates are relatively low [*Koerner*, 1979] and this effect is less marked. A slightly different threshold-based melt detection technique was therefore used to map melt on the Greenland ice sheet:

$$M_1 = W_{mn} - a \quad (1)$$

$$M_2 = W_{mn} - b \quad (2)$$

Here, a and b are user defined constants. Using trial and error and the available air temperature records, the optimal values for a and b were identified as: a = 2.0, b = 3.0 dB. For each pixel, all periods when either (1) σ^0 remained below M_1 for 2 or more consecutive days, or (2) σ^0 dropped below M_2 for 1 d, were categorized as melt days. Step 1 eliminates possible "false starts" in melt onset; and step 2 makes it possible to capture short periods of melt at high elevations on the ice sheet. These thresholds work well for most of the pixels. However, for some pixels (∼2.6% of all pixels) in the south and west of Greenland where the winter accumulation rates are high, σ^0 may decrease substantially during the winter, with the result that the end of winter (premelt) σ^0 is already below the melt detection threshold. For these pixels, more stringent thresholds (a_2 = 3.0, b_2 = 3.5) were used to avoid the false detection of melt onset. The dates of melt onset and freeze up in each pixel were

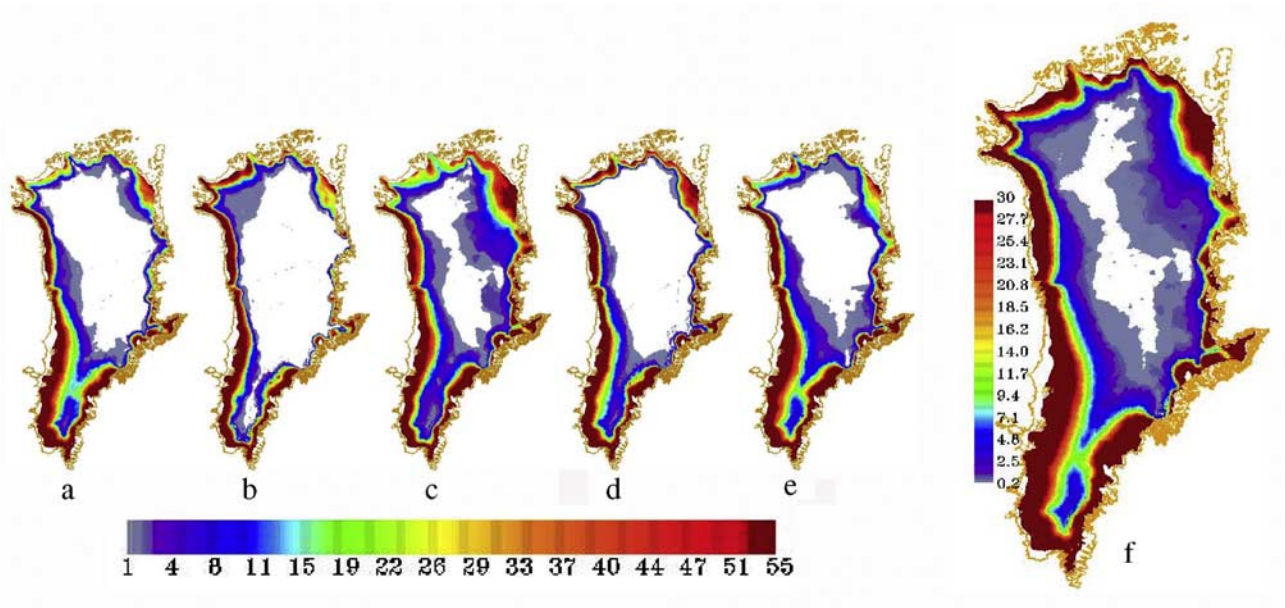

Figure 3. Melt extent and duration (number of days) in (a) 2000, (b) 2001, (c) 2002, (d) 2003, (e) 2004, and (f) the 5-a mean. Regions which experienced no melt in a particular year are shown in white.

taken as the first melt day and the last melt day plus one, respectively. The annual melt duration in each pixel was defined as the time period between melt onset and freeze up minus the duration of any melt-free periods within the melt season.

[19] In addition to the observations from ETH and CP1, air temperature records for the period 2000–2003 from Dye-2, NASA-SE, and Tunu-N (all of which are located in the saturation/percolation zone of the ice sheet) were used to validate the estimates of melt duration from QSCAT. There is a close correspondence between the melt durations derived from the QSCAT data (MD_{QS}) and positive air temperatures in the 1100–2000 time window (MD_T). A linear regression gives $MD_{QS} = 1.08\ MD_T + 3.7$ d ($r^2 = 0.94$, $P < 0.001$, standard error of the estimate of 7.9 d). There is also a good relationship between MD_{QS} and the annual positive degree-day total ($\Sigma PDD = 0.88 + 0.2542\ MD_{QS} + 0.0135\ MD_{QS}^2$, $r^2 = 0.95$, $p < 0.001$, standard error of the estimate = 12.8 PDD). This implies that the melt season duration estimated from QSCAT is longer than that derived from the air temperature records. There are three possible reasons for this: (1) melt occurred under subfreezing near surface air temperature conditions, which is most likely at high elevations where the atmosphere is thinner, and under clear sky conditions when short-wave radiation receipts at the ice surface are high, (2) QSCAT still detects subsurface meltwater when the ice surface freezes due to a sudden drop of the near surface air temperature to below the melting point, and (3) the melt thresholds are insufficiently conservative and the melt season duration was overestimated using QSCAT data.

[20] Since there are no field measurements of snow wetness, it is not possible to directly estimate the accuracy of the melt season duration estimated from QSCAT using the chosen thresholds. However, the regression analyses indicate that the estimated melt season durations are well correlated with the air temperature observations and we take the standard error of the regression estimate as a measure of the uncertainty associated with our estimates of melt duration.

[21] *Ashcraft and Long* [2006] compared the results of six different methods (based on either σ^0 or passive microwave brightness temperatures) used to detect melt over Greenland in the year 2000. Three of the methods used a simplified melt event model for melt detection. These "α-based" methods are similar to the method used in this study because they use melt detection thresholds based on microwave attenuation in the wet snow layer. Ashcraft and Long found that the α-based methods were consistent in their assessment of the timing and location of surface melt. This strengthens our argument that the estimates of melt extent and duration generated in this study are suitable for use in analyses of the spatial and temporal distributions of surface melt over the ice sheet and their relationship to climatic variability during the study period.

4.3. Melt Results, 2000–2004

4.3.1. Melt Extent and Duration

[22] Only σ^0 measurements flagged as useable in the QSCAT L1B files are included in the SIR product [*Long and Hicks*, 2005]. There are 4 d during the study period

Table 1. Mean Melt Extent and Mean Melt Duration Over the Greenland Ice Sheet as a Whole During the Period 2000–2004

Year	Melt Extent, %	Melt Duration for All Cells, d	Melt Duration for Melt Cells, d	Maximum Melt Extent,[a] %
2000	54.9	16.0	28.8	60.0
2001	44.2	14.3	32.1	50.1
2002	79.7	20.5	25.7	81.9
2003	48.2	18.6	38.1	54.0
2004	64.0	19.4	30.0	68.2

[a]The melt extent calculated on the assumption that all bare ice and mixed pixels melted on at least 1 d each year is given.

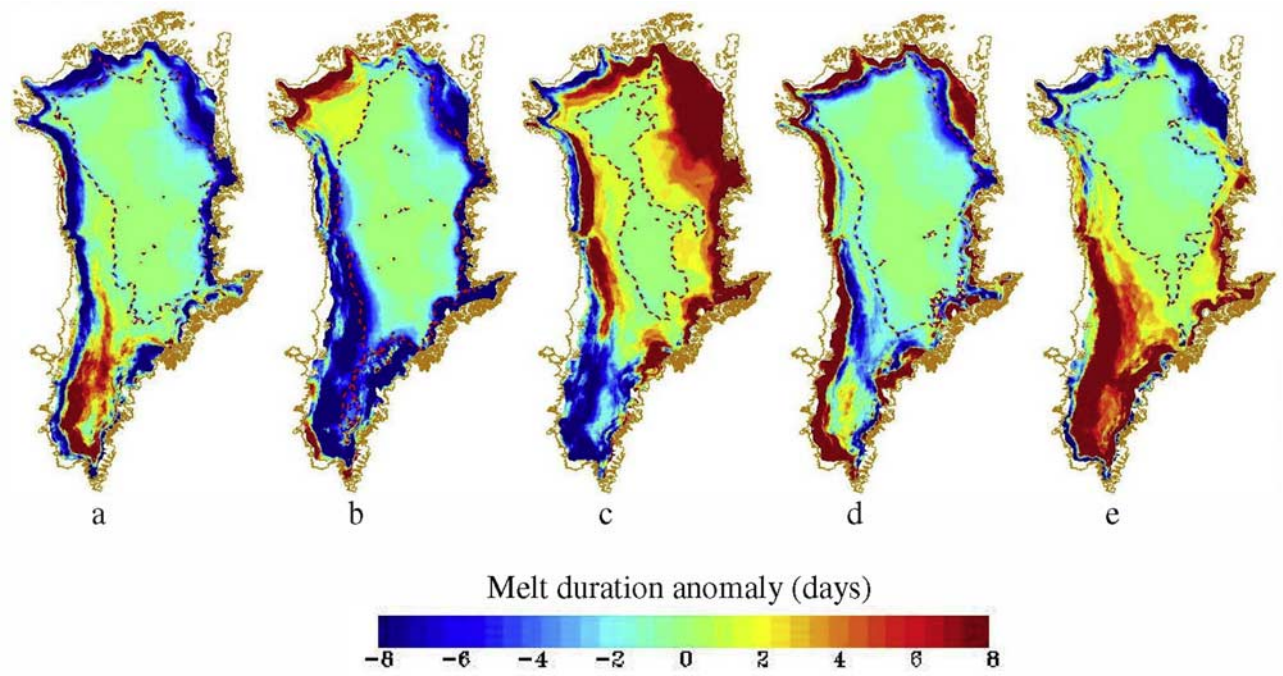

Figure 4. Anomalies in melt duration (days) relative to the 2000–2004 mean for the summers of (a) 2000, (b) 2001, (c) 2002, (d) 2003, and (e) 2004, with dashed contours outlining regions that experienced no melt in that year.

with missing data: days 132, 133, and 188 in 2001, and day 228 in 2003. The backscatter for these days was calculated by linear interpolation from adjacent days. Figure 3 shows the annual and average melt extents and durations for the 2000–2004 period. The maximum melt extent occurred in 2002, and the minimum in 2001. The percentage of the ice sheet that experienced melt for at least 1 d in a given year was calculated from the ratio of the melt area to the total area (Table 1). Percentages calculated on the assumption that all bare ice and mixed pixels experienced melt on at least 1 d in each year are given Table 1; 2002 had the most extensive melt within the 5-a period (79.7%), and 2001 had the least extensive (44.2%).

[23] Figure 4 shows the melt season duration anomalies in each year relative to the 5-a mean (Figure 3f). There was an extremely positive melt anomaly in 2002 over west, east, and northeast Greenland (north of 66°N). In the south dome region of the ice sheet the longest melt season was in 2004 (Figures 3e and 4e). In 2001, melt anomalies were negative over most of Greenland except for the northwest corner, where melt extended to higher elevations than in any other year of the 5-a period (Figure 4b). The mean melt duration over the ice sheet in a given year was calculated for (1) all cells, and (2) all cells that experienced melt in that year. The mean melt duration (for all cells) was longest in 2002 (20.5 d) and shortest in 2001 (14.3 d), which is consistent with the measurements of melt extent. However, the mean melt duration for melt cells was shortest in 2002 (25.7 d). This is due to the fact that the large melt extent in 2002 was mainly attributable to a period of widespread melt over high elevation areas of west, east, and northeast Greenland that lasted for only a few days (Figure 3c) [*Tedesco*, 2007]. For melt cells, the mean melt duration was longest in 2003, which is consistent with the air temperature observations at the AWS sites (not shown) and the fact that the low elevation regions of the ice sheet had extremely positive melt duration anomalies in 2003 (Figure 4d).

[24] Of the 78708 cells, 68181 experienced melt for at least 1 d during the 2000–2004 period. The total area affected by melt was 1.36×10^6 km^2, or 86% of the area of the ice sheet. This excludes the area of the bare ice mask and mixed pixels, most of which probably experienced melting each year. If these were included, the total area affected by melt would be 1.53×10^6 km^2 (88%). The average melt duration decreases rapidly as elevation increases from the ice margin to the high interior (Figure 3f). To a first approximation, areas above 2000 m in the north and 2500 m in the central and south dome areas of the ice sheet experienced less than 4 d of melt on average (grey to purple region in Figure 3f). On average, 55% of the melt area experienced melt for less than 1 week each year (grey to cyan region in Figure 3f), and about 76% of the melt area experienced less than 30 d of melt (grey to the upper limit of the dark red region in Figure 3f). Only 13% of the melt region experienced more than 60 d of melt.

[25] Figure 5 shows the 5-a mean melt duration, melt distribution, and melt occurrence within each elevation band. The melt distribution is defined as the percentage of all melt pixels that occurred within each elevation band, and the melt occurrence as the percentage of the pixels within an elevation band that experienced melt. The melt duration decreases as the elevation increases, and it decreases more rapidly above 1400 m than at lower elevations. The melt distribution curve shows that there are more melt pixels at high elevations (>1800 m) than at low elevations. This reflects the facts that the central part of the ice sheet lies at

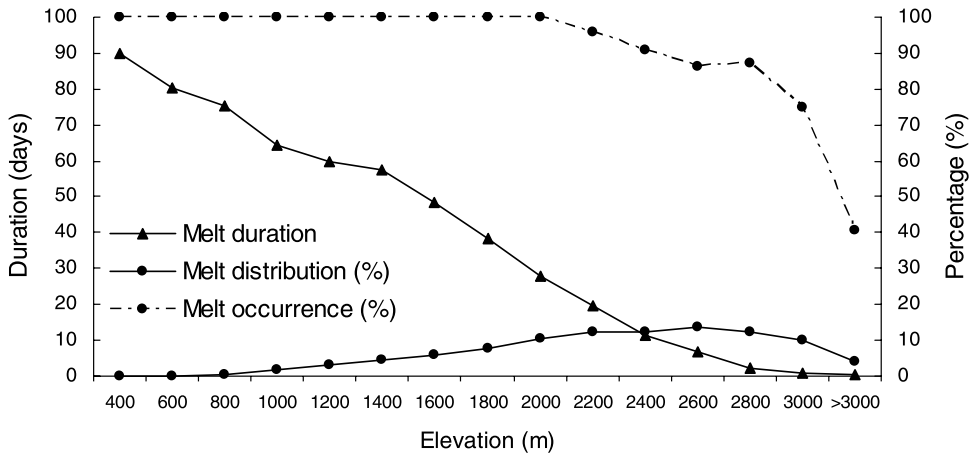

Figure 5. Average melt duration, distribution, and occurrence within each elevation band. The melt distribution was calculated as the percentage of melt pixels within each elevation band in relation to the total number of melt pixels over the Greenland ice sheet (68181). The melt occurrence was calculated as the percentage of melt pixels in relation to the total number of pixels within an elevation band.

3000 m or more above sea level, that 87% of the ice sheet is above 1,220 m asl [*Putnins*, 1970], and that most pixels at low elevations were excluded from the analysis, either because they were mixed pixels or because they were located in the bare ice zone. All pixels below 1800 m experienced melt (melt occurrence = 100%). Even for elevation bands as high as 2800–3000 m, nearly 75% of pixels experienced melt during the study period.

[26] Stepwise regression indicates that the spatial pattern of the 5-a mean melt duration can be well explained in terms of surface elevation and latitude: $MD_{QS} = 364.69 - 0.0435h - 3.434y$ ($r^2 = 0.76$, $p < 0.0001$), where h is surface elevation (m), and y is latitude (degrees north). The r^2 increases by only 0.002 when longitude is included in the regression analysis. The correlation with elevation alone is −0.64, while that with longitude is −0.18 and that with latitude is −0.38. Thus surface elevation and latitude appear to be the main influences on mean melt duration on the Greenland ice sheet.

4.3.2. Seasonal Melt Cycle

[27] To illustrate the seasonal cycle of surface melt, the daily melt extent was calculated for the period May to October of each year. Figure 6 depicts the distribution and occurrence of melt in each month from May to October. The melt occurrence was calculated as the average percentage of days with melt in each of these months over the 2000–2004 period. On average, melt starts in the middle of May along the west and southeast coasts. In early June, melt begins to spread and the melt extent increases rapidly, reaching its peak in late June to mid-July. From mid-July, freeze up begins to occur on the north and east flanks of the ice sheet and the areal extent of melt begins to decrease. Melt ceases

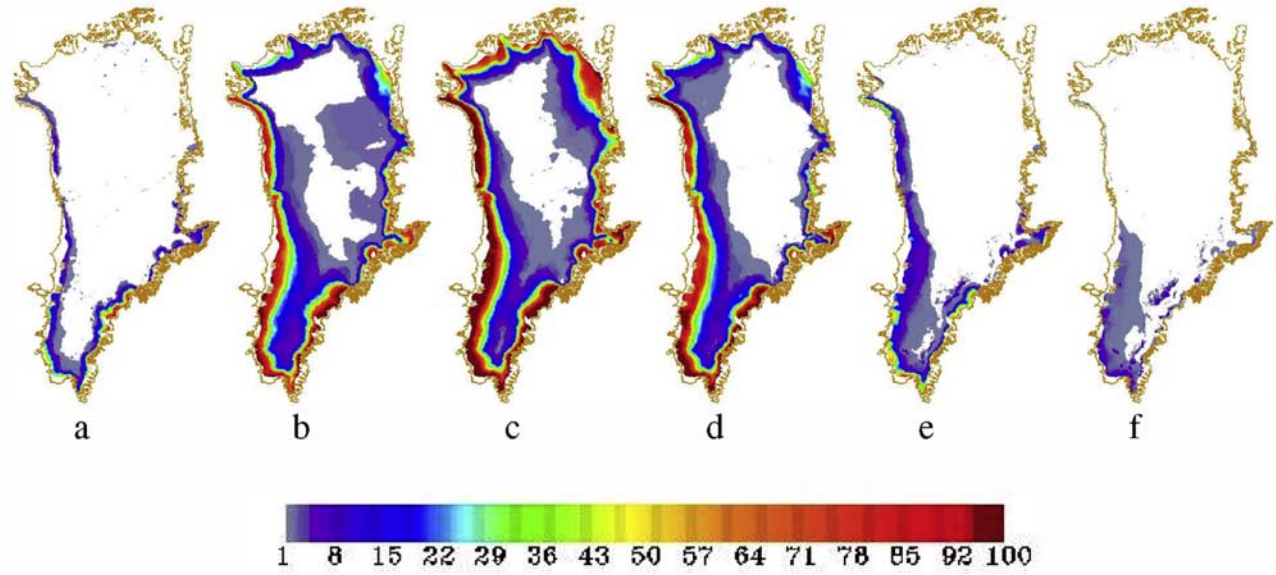

Figure 6. Monthly mean melt extent and occurrence (%) in (a) May, (b) June, (c) July, (d) August, (e) September, and (f) October. White represents areas that experienced no melt in that month.

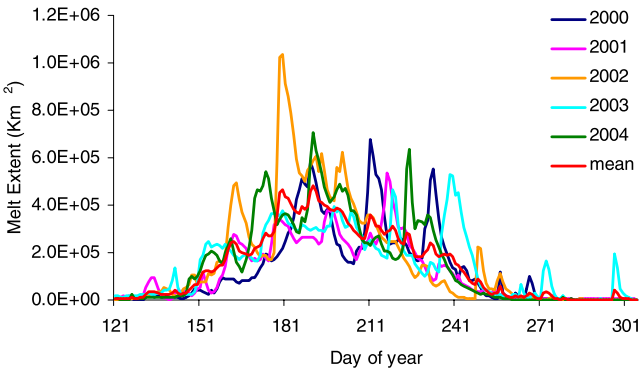

Figure 7. Daily melt extent (km^2) from May to October for the 2000–2004 period.

over most of the ice sheet by the end of September, but there is still some melt in southern Greenland in October, especially in the west. This is largely due to the prolonged melt in 2003. Although the melt extent is similar in June and July (Figures 6b and 6c), the melt occurrence is much higher in July than in June for low elevation areas.

[28] Figure 7 shows the progression of melt extent in each individual summer and the mean for the 5-a period. Each year is characterized by a background seasonal cycle on which up to 5 or 6 melt events of a few days duration are superimposed. The melt extent can fluctuate considerably during these events, the timing of which varies from year to year. This will be discussed further later.

4.3.3. Regional Differences in Surface Melt

[29] In order to examine the regional variability of melt extent and duration, the Greenland ice sheet was divided into nine regions defined by topography. Because of differences in the orientation of topographic barriers relative to the major streamlines of airflow over the ice sheet and the distribution of warm air sources, these barriers play an important role in dividing the ice sheet surface into different climatic zones [*Mote and Anderson*, 1995; *Ohmura and Reeh*, 1991]. The nine regions are similar to those defined by *Ohmura and Reeh* [1991], although two of their larger regions, Jakobshavn and Angmagssalik, were subdivided into smaller regions to conform with the higher spatial resolution of this study (Figure 1). The mean melt duration in each of the nine regions was calculated for each summer for the 2000–2004 period (Table 2). The percentage of the ice sheet in each region that is excluded from the calculation because it consists of either bare ice or mixed pixels is given in Table 2. In general, the melt duration is longer for regions in west Greenland (regions 1, 2, 3, and 4) than for regions at similar latitudes in east Greenland (regions 6, 7, 8 and 9), and melt duration decreases from south to north. This is consistent with the conclusion of *Steffen and Box* [2001] that the climate on the eastern side of Greenland is colder than that on the western side at the same latitude. Region 1, in the southwest corner of Greenland, has a relatively low mean elevation (2035 m) and the longest mean melt duration (68.2 d). Region 7, which includes the highest regions of the ice sheet, has the highest mean elevation (2840 m) and the shortest mean melt duration (7.0 d). Although 2002 had the most extensive melt extent and duration in the 2000–2004 period for the ice sheet as a whole (Table 1), only three regions on the eastern side of the ice sheet (regions 6, 7, and 8) had their maximum melt duration in 2002. Regions in the south and southwest had their maximum melt duration in either 2003 (region 1) or 2004 (regions 2, 3, and 9). Although regions 2, 3, and 6–9 all had their minimum melt durations in 2001, region 5, in the northernmost part of Greenland, had its maximum melt duration in 2001. This demonstrates the highly variable characteristics of surface melt over the different regions of the ice sheet.

[30] The percentage of each region of the ice sheet that was melting on each day of the year during the period 2000–2004, and the 5-a mean for each region, is shown in Figure 8. The southern regions (region 1, 2, 3, and 9) have the longest melt seasons, extending from early May to late October. The northernmost region (5) and the northeast region (6) have the shortest melt seasons and are the last to start melting, and the earliest to freeze up. The standard deviation (SD) curves in Figure 8 show the interannual variability of the daily melt extent from 2000–2004. Region 1, where most pixels experienced melt every summer, has the lowest SD, while region 6, where most pixels only experienced melt in very warm years, like 2002, has the highest SD.

4.4. Influence of Atmospheric Conditions on Surface Melt Patterns

[31] To investigate the relationships between atmospheric conditions and the extent and duration of surface melt, correlations with the monthly mean geopotential height from May to August during the 2000–2004 period (as derived from the National Centers for Environmental Pre-

Table 2. Mean Melt Season Duration in the Nine Regions of the Ice Sheet[a]

Region	2000	2001	2002	2003	2004	Mean	SD	Elevation, m	Percentage, %
1	70.2	61.3	58.1	80.1	71.3	68.2	8.7	2035	25.0
2	45.5	33.7	35.2	45.7	49.5	41.9	7.1	2242	11.9
3	21.2	16.9	22.4	22.1	27.6	22.0	3.8	2359	10.7
4	12.4	13.6	16.8	16.7	15.4	15.0	1.9	2259	4.2
5	7.0	13.8	11.3	11.7	8.3	10.4	2.8	1817	11.5
6	4.9	4.4	17.0	7.6	6.1	8.0	5.2	2198	8.6
7	4.8	3.5	10.8	7.0	8.8	7.0	3.0	2840	5.1
8	16.1	9.2	22.7	17.8	20.9	17.3	5.2	2633	22.0
9	34.6	28.5	35.2	35.1	40.7	34.8	4.3	2283	11.0

[a]Melt season duration is given in days. The 5-a mean duration, standard deviation, the mean elevation (m above sea level (asl)), and the percentage of the ice sheet that is excluded from melt detection (bare ice and mixed pixels) in each region is also included.

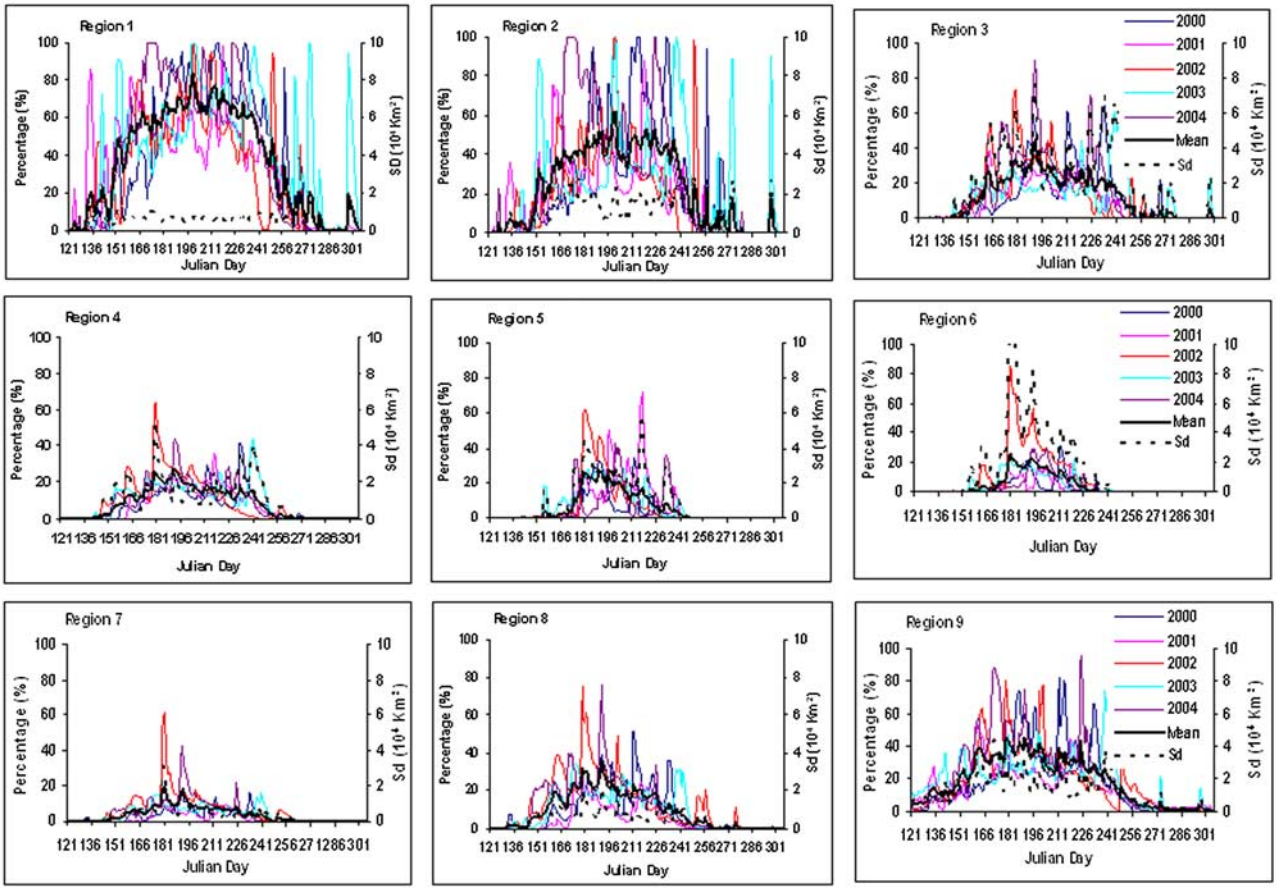

Figure 8. Annual and mean daily percentage of each region of the ice sheet that was melting as a function of day of year during the period 2000–2004. The dashed black lines represent the standard deviation of the mean.

diction/National Center for Atmospheric Research (NCEP/NCAR) Reanalysis 1 [*Kalnay et al.*, 1996]) were calculated for each of the nine topographic regions on the Greenland ice sheet. To find the pressure level that correlates most strongly with the surface melt, separate correlation analyses were conducted for the 700 hPa, 500 hPa, and 300 hPa pressure levels (Table 3). Geopotential height at the 300 hPa pressure level, the upper troposphere, correlates most strongly with surface melt on the Greenland ice sheet. In general, geopotential height at all three pressure levels is better correlated with the monthly mean melt duration than with melt extent. This suggests that melt duration might be a better index of climatic conditions over the ice sheet than the more widely used parameter, melt extent [e.g., *Abdalati and Steffen*, 1997, 2001; *Mote*, 1998a, 1998b]. The correlation coefficients between daily melt extent and 300 hPa geopotential height for each region are reported in Table 3 and are similar to those derived from the monthly analyses.

[32] Figure 8 clearly shows a distinct melt event that affected all the regions except regions 1 and 2 during the period 27 June to 2 July (days 178–183), 2002. During this event, melt reached the highest elevations on the northeast side of the ice sheet (region 6) during the 2000–2004 period. This melt event was also observed using Special Sensor Microwave Imager (SSM/I) brightness temperature daily variations [*Tedesco*, 2007]. Synoptic analysis indicates that this event was associated with the intrusion of a ridge of high pressure over the ice sheet from the North Atlantic Ocean. Warm air advection by strong southerly flow associated with this ridge of high pressure is the most likely cause of the extensive melt on the ice sheet.

Table 3. Correlation Coefficients Between Monthly Mean Melt Duration or Melt Extent and Geopotential Height at the 700, 500, and 300 hPa Pressure Levels in the Nine Regions of the Ice Sheet[a]

	700 hPa		500 hPa		300 hPa		
Region	MD	ME	MD	ME	MD	ME	300 hPa Daily ME
1	0.86	0.79	0.93	0.86	0.94	0.86	0.79
2	0.77	0.78	0.87	0.87	0.89	0.89	0.73
3	0.60	0.56	0.76	0.70	0.80	0.73	0.77
4	0.62	0.49	0.81	0.69	0.91	0.81	0.80
5	0.52	0.55	0.68	0.73	0.73	0.78	0.69
6	0.33	0.36	0.53	0.59	0.59	0.66	0.62
7	0.48	0.40	0.70	0.59	0.75	0.62	0.69
8	0.53	0.46	0.71	0.62	0.77	0.67	0.71
9	0.70	0.66	0.79	0.76	0.80	0.79	0.75
Mean	0.60	0.56	0.75	0.71	0.80	0.76	0.73

[a]MD, monthly mean melt duration; ME, melt extent. The correlation coefficients of daily melt extent and 300 hPa geopotential height during the 2000–2004 period are given.

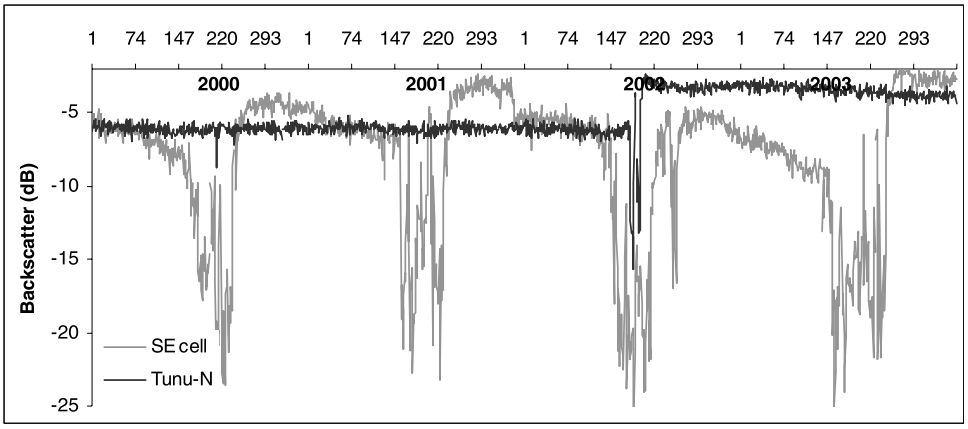

Figure 9. Time series of QSCAT σ^0 for Tunu-N and one cell in the southeastern (SE) corner of Greenland (see locations in Figure 1) during the 2000–2003 period.

4.5. Comparisons With Other Microwave Melt Detection Methods and Results

[33] QSCAT data have been used to detect the extent and duration of surface melt on the Greenland ice sheet in previous studies [*Nghiem et al.*, 2001; *Steffen et al.*, 2004]. *Steffen et al.* [2004, Figure 4] detected surface melt using a diurnal variation method (Q-DV) and raw resolution QSCAT data (25 km). Maps of the melt extent and duration for the period 2000–2003 [*Steffen et al.*, 2004, Figure 4] are similar to those shown in Figure 3 for the same 4 a. The maximum melt extent in 2002 is larger in their map than in ours. We suspect that this is probably related to the lower temporal resolution and timing of the enhanced SIR product. The overpass times of the raw QSCAT data used by *Steffen et al.* [2004] are about 6:00 for ascending and 18:00 for descending passes. However, the effective measurement times are 11:00 to 20:00 for the descending pass SIR images used in this study. Thus the SIR product may not detect short melt events at high elevations that occurred only in the late afternoon. Overall our maps are less noisy and show a finer melt duration pattern than their maps, this is likely due to the averaging involved in the enhanced resolution SIR product.

[34] *Ashcraft and Long* [2006] compared six different melt detection methods based on either σ^0 or passive microwave brightness temperatures over Greenland for the year 2000. They found good spatial and temporal correlations between the melt patterns detected by the 3 α-based methods. One of these methods (the Q-α method) is very similar to the method employed in this study. *Ashcraft and Long* [2006] used a single threshold (3 dB below the winter mean backscatter) to detect melt, while we used two thresholds in this study. Nevertheless, the extent of melt derived for the year 2000 using the two methods was very close: 58% of the ice sheet for Q-α method of *Ashcraft and Long* [2006, Table 2], and 60% in this study (in Table 1). The small difference of 2% may be due to the difference in the spatial resolution of the QSCAT data used in the two studies: 8.9 km in Q-α, 4.45 km in this study. Compared to the α-based methods, the Q-DV method underestimated melt duration considerably, especially at low elevations, because it is based on a sufficient but not a necessary condition for melt detection [*Ashcraft and Long*, 2006].

[35] Greenland melt extent has also been measured using passive microwave data [e.g., *Mote and Anderson*, 1995; *Abdalati and Steffen*, 1995, 1997; *Tedesco*, 2007]. Compared to passive microwave sensors, such as the SSM/I, QSCAT is more sensitive to melt and detects a larger melt extent on the ice sheet during the same period [*Steffen et al.*, 2004; *Tedesco*, 2007]. However, *Ashcraft and Long* [2006] indicated that different melt detection methods applied to the same sensor can derive very different estimates of melt extent and duration. Therefore caution should be exercised when comparing results from the different methods and sensors.

5. Interannual Changes in the Distribution of Ice Layer Formation

5.1. Ice Layer Formation: Signature and Detection

[36] Figure 2 shows a 4-a time series of QSCAT σ^0 at three AWS locations. At CP1, (Figure 2a) there were obvious jumps in σ^0 between the periods immediately before and after the 2001 and 2002 melt seasons. *Nghiem et al.* [2005] observed a similar phenomenon in 2002 at the NASA-E weather station (see location in Figure 1). At NASA-E, field observations confirmed that the main cause of the σ^0 jump was a 2-cm-thick ice layer in the snowpack and a number of vertical percolation features. As snow accumulates in the following winter, these ice layers become buried and their contribution to σ^0 becomes weaker because of two-way attenuation of the microwave signal in the snow [*Nghiem et al.*, 2005]. This explains the decrease in σ^0 over the winter (Figure 2a), the magnitude of which appears to depend on the amount of snow accumulation. For low accumulation areas, such as the northeast of Greenland [*Ohmura and Reeh*, 1991; *Bales et al.*, 2001], the over-winter decrease in σ^0 is negligible. For example, at Tunu-N (Figure 9), σ^0 increased from $\sim$−6.0 dB to $\sim$−3.0 dB over the summer of 2002 because of ice layer formation during that summer, but it decreased by only about 0.8 dB over the winter of 2002–2003. For areas such as the southeastern corner of Greenland, where the snow accumulation is greatest [*Ohmura and Reeh*, 1991; *Bales et al.*, 2001], the over-winter decrease of σ^0 is much larger, though variable

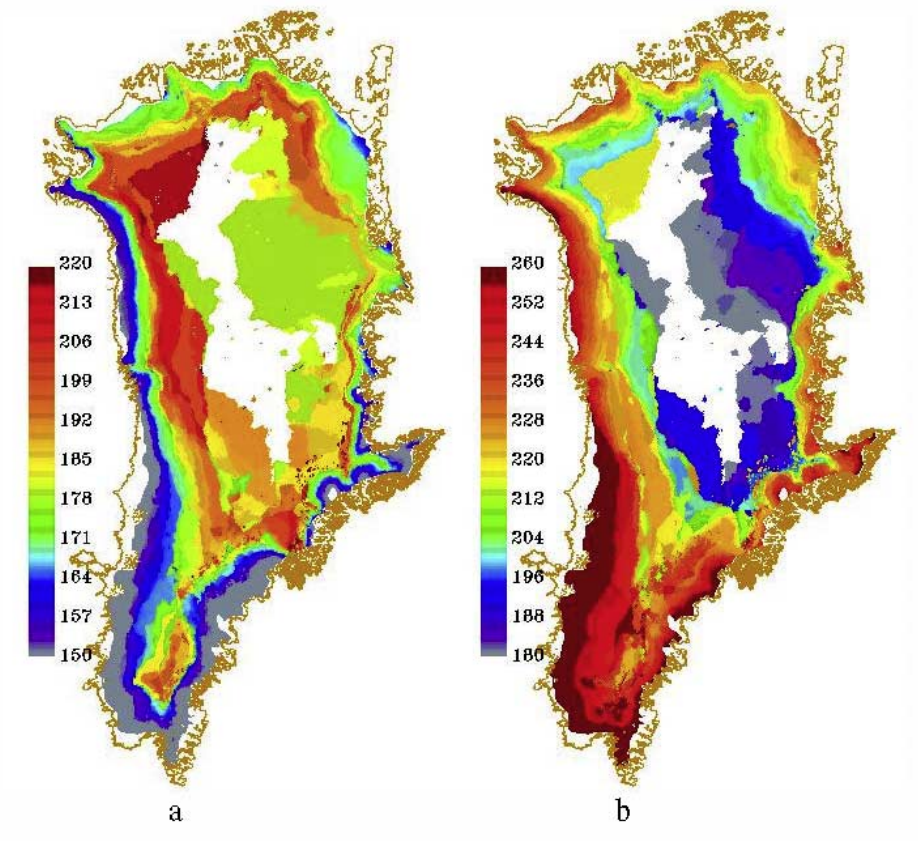

Figure 10. (a) Average melt onset dates and (b) melt freeze up dates during the 2000–2004 period. Dates are given in terms of day of year, and the averages at each pixel were calculated using all melt onset/freeze up dates for years when melt occurred in the pixel. White represents areas that experienced no melt during the 5-a period.

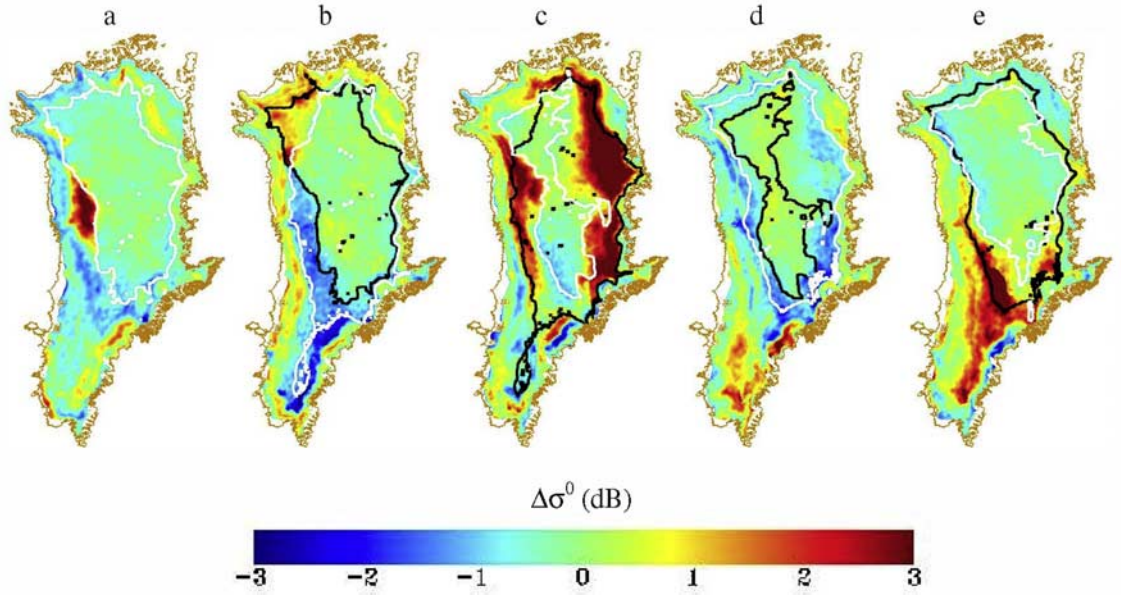

Figure 11. Changes in the biweekly averaged backscatter between the freeze up periods in the current and the previous fall in (a) 2000, (b) 2001, (c) 2002, (d) 2003, and (e) 2004. The solid white and black contours represent the upper limits of melt for the current and the previous summers, respectively.

(Figure 9). It was ~2.0 dB over the 2000–2001 winter, and ~5.0 dB over the 2002–2003 winter.

[37] *Nghiem et al.* [2005] developed the first algorithm to detect ice layer formation on the Greenland ice sheet. Their approach was to subtract the biweekly averaged backscatter for a period before a melt season from the biweekly averaged backscatter for a period after the same melt season to determine the backscatter change. A possible limitation of this approach is that, in many regions, σ^0 may change between the end of one melt season and the start of the next because of attenuation by winter snow accumulation. Since the magnitude of attenuation is probably a function of the magnitude of over winter snow accumulation, this implies that the magnitude of ice layer formation suggested by the over-summer change in σ^0 will be a function of the end of winter σ^0, and hence of the over-winter snowfall. Another possible limitation of the Nghiem approach is that fixed dates were used to mark the start and the end of the melt season, when in reality these dates can vary considerably. Figures 10a and 10b show the average melt onset dates and freeze up dates, respectively, over the ice sheet during the 2000–2004 period (the averages for each pixel were calculated using all melt onset (freeze up) dates for years when melt occurred in the pixel). From the ice sheet margin to the high interior, melt onset dates ranged from ≤day 150 (~the end of May) to ≥day 220 (~beginning of August). The freeze up dates ranged from ≤day 180 (~the end of June) at the highest elevations to ≥day 260 (approximately mid-September) at the lowest elevations. Thus the use of fixed melt onset/freeze up dates to define the melt season for the whole ice sheet will result in some bias in the derived extent of ice layer formation (because σ^0 may not have reached its end of winter minimum at some sites by the date chosen to define the start of the melt season, while at other sites it may have decreased from its end of summer value by the date taken to define the end of the melt season).

[38] To avoid these problems, a different approach was used to identify changes in the distribution of ice layer formation in this study. This approach compares the magnitude of σ^0 between biweekly periods starting two weeks after the end of successive melt seasons, and assumes that the larger the increase in σ^0 between successive melt seasons, the greater the increase in ice layer formation between the two melt seasons. Where σ^0 decreases between melt seasons, this implies reduced ice layer formation in melt season 2. For the purposes of these calculations, actual freeze up dates for each pixel were used instead of fixed dates to determine the timing of the end of each melt season. For pixels that experienced no melt in a given melt season, a fixed date, 31 October was chosen as the reference date, and the biweekly averaged σ^0 was determined for those pixels as well.

5.2. Changes in the Distribution of Ice Layer Formation, 2000–2004

[39] Maps of the changes in the biweekly averaged σ^0 in each of the 78708 cells between successive end of melt season periods for the years 2000–2004 are shown in Figure 11. The solid white and black contours represent the upper limits of melt for the current and the previous summers, respectively. The yellow to red represent regions where there was an increase in backscatter from ice layers in the snowpack relative to the previous fall. The darker the red, the larger is the increase in backscatter. Typically, large increases in backscatter occur in regions where the upper limit of melt in the current summer lies inside the limit in the previous summer (for example, the extensive region that encircles much of the northern part of the ice sheet in 2002 (Figure 11c)). The cyan to blue represent regions with decreased backscatter. Typically these are regions where the upper limit of melt in the previous summer lies above the upper limit of melt for the current summer (for example, the region that runs north-south along the western side of Greenland in 2001 (Figure 11b)). Figure 11 reveals significant variations in the extent and distribution of new ice layer formation during the 2000–2004 period. Melt duration maps (Figure 3) indicate that ice layers can be formed with only a few days of melt in most areas of the percolation zone.

[40] Overall, the most extensive increase in the area of ice layer formation in the west, east, and northeast of Greenland occurred in 2002, while in southern Greenland it occurred in 2004. The largest decrease in the area of ice layer formation over most regions of the ice sheet occurred in 2001, but there was a considerable increase in the area of ice layer formation in those parts of the northwest corner of Greenland where melt only occurred in that year. In 2003, there were clear decreases in σ^0 in areas where there had been increases in the area of ice layer formation in 2002. This is consistent with the reduced melt extent in these areas in 2003. These large interannual variations in the distribution of regions of ice layer formation could result in significant variations in near surface firn density that should be accounted for in the estimation of mass change from altimeter measurements.

6. Summary and Conclusions

[41] Time series of enhanced resolution QSCAT backscatter allow the detection of summer melt on the Greenland ice sheet at a higher spatial resolution than was possible in previous studies. The results reveal large temporal and spatial variability in the occurrence of surface melt on the ice sheet in the period 2000–2004. Although melt occurred over 86% of the ice sheet during the study period, nearly 55% of the melt areas experienced melt for less than 1 week each year. The extensive melt that occurred in the summer of 2002 was largely due to a single high melt event that lasted for only a few days. This event was associated with the intrusion of a ridge of high pressure over the ice sheet from the North Atlantic Ocean. Warm air advection by strong southerly flow associated with this ridge is the most likely cause of the extensive melt on the ice sheet. The mean melt extent in each region of the ice sheet was positively correlated with the local 300 hPa geopotential height at both daily and monthly timescales. However, the monthly mean melt duration was more strongly correlated with the local geopotential height at all pressure levels than was the melt extent. This suggests that melt duration may be a more useful index than melt extent of the influence of atmospheric conditions and climate change on melt on the ice sheet. The strong relationship between annual melt duration and local positive degree day total suggests that maps of annual melt duration could be used to derive PDD fields that would

be useful for validation of regional climate model simulations and as input to calculations of summer melt volume using temperature index models.

[42] Interannual changes in the distribution of ice layers formed by refreezing of meltwater within snow and firn in the percolation zone of the ice sheet were mapped using the change of biweekly averaged backscatter between the freeze up periods in successive falls. The results indicate that ice layers can be formed after only a few days of melt. Extensive increases in the area of ice layer formation were detected in the summer of 2002, which is consistent with the occurrence of maximum melt extent at high elevations of the ice sheet in that year. Such changes are probably closely related to changes in the rate of densification of near surface snow and firn, and may be associated with changes in surface height that are not indicative of mass balance changes [*Braithwaite et al.*, 1994]. The distribution of ice layers in snow and firn may also be an important influence on the performance of satellite radar altimeters over ice sheets and on the accuracy of surface elevation retrievals [*Davis and Ferguson*, 2004; *Thomas et al.*, 2006]. A recent study [*Thomas et al.*, 2006] indicated that the rate of thickening estimated from ERS radar altimeter measurements (1992–2002/2003) for high elevation regions (>1500 m) of Greenland was greater than that estimated from ICESat/Airborne Topographic Mapper laser altimeter data (1993/1994–2004) over nearly the same time interval. This may be a result of increased surface melting in warm summers (e.g., 2002) extending the upper limit of the percolation zone to higher elevations, and a consequent lifting of the radar-reflecting ice layers within near-surface snow [*Scott et al.*, 2006a, 2006b; *Thomas et al.*, 2006]. Systematic mapping of ice layer formation over Greenland may therefore have an important role to play in the interpretation of altimeter-derived measurements of changes in the surface elevation of the ice sheet.

[43] The extent and duration of surface melt estimated in this study are consistent with results from previous studies based on QSCAT data [*Steffen et al.*, 2004; *Ashcraft and Long*, 2006]. Use of the enhanced resolution QSCAT SIR product provides more detailed information about melt patterns than can be obtained using the raw data. However, the temporal averaging involved in producing the descending pass SIR product may introduce some bias (underestimation) of melt extent and duration. This bias might be minimized by using SIR products generated according to local pass times (morning/evening) instead of ascending/descending passes [*Hicks and Long*, 2005]. The Ku band QSCAT scatterometer proves to be very effective in detecting surface melt and changes in the distribution of ice layer formation on the Greenland ice sheet. Long-term acquisition of backscatter data from this (or a similar) instrument would be very valuable for detecting changes in surface mass balance of the ice sheet.

[44] **Acknowledgments.** The Meteorological Service of Canada (CRYSYS program) and the Canadian Foundation for Climate and Atmospheric Sciences (Polar Climate Stability Network) supported this work. We are very grateful to Thomas Mote for his insightful comments on the manuscript, to Alex Gardner for his help with the atmospheric circulation analysis in the study, Bea Csatho for providing an outline of the Greenland ice sheet (originally provided by Simon Ekholm, Kort-og Matrikelstyrelsen (KMS, National Survey and Cadastre, Denmark)), and to D.G. Long for his help with the QSCAT data. We thank Adrian Luckman and an anonymous reviewer for helpful comments on an earlier version of the paper. The Microwave Earth Remote Sensing Laboratory, Brigham Young University provided the QSCAT data.

References

Abdalati, W., and K. Steffen (1995), Passive microwave-derived snowmelt regions on the Greenland ice sheet, *Geophys. Res. Lett.*, *22*, 787–790.

Abdalati, W., and K. Steffen (1997), Snowmelt on the Greenland ice sheet as derived from passive microwave satellite data, *J. Clim.*, *10*, 165–175.

Abdalati, W., and K. Steffen (2001), Greenland ice sheet melt extent: 1979–1999, *J. Geophys. Res.*, *106*, 33,983–33,988.

Ashcraft, I. S., and D. G. Long (2006), Comparison of methods for melt detection over Greenland using active and passive microwave measurements, *Int. J. Remote Sens.*, *27*, 2469–2488.

Bales, R. C., J. R. McConnell, E. Mosley-Thompson, and G. Lamorey (2001), Accumulation map for the Greenland Ice Sheet: 1971–1990, *Geophys. Res. Lett.*, *28*, 2967–2970.

Benson, C. S. (1962), Stratigraphic studies in the snow and firn on the Greenland ice sheet, *Res. Rep. 70*, Snow, Ice, Permafrost Res. Estab., U.S. Army Corps of Eng., Hanover, N. H.

Bindschadler, R. (1998), Monitoring ice sheet behavior from space, *Rev. Geophys.*, *36*, 79–104.

Braithwaite, R. J., M. Laternser, and T. W. Pfeffer (1994), Variations of near-surface firn density in the lower accumulation area of the Greenland ice sheet, Pakitsoq, West Greenland, *J. Glaciol.*, *40*, 477–485.

Brown, J., O. J. Ferrians Jr., J. A. Heginbottom, and E. S. Melnikov (1998), Circum-arctic map of permafrost and ground ice conditions, World Data Cent. for Glaciol., Boulder, Colo.

Cazenave, A., and R. S. Nerem (2004), Present-day sea level change: Observations and causes, *Rev. Geophys.*, *42*, RG3001, doi:10.1029/2003RG000139.

Church, J. A., et al. (2001), Changes in sea level, in *Climate Change 2001: The Scientific Basis*, edited by J. T. Houghton et al. pp. 639–693, Cambridge Univ. Press, New York.

Comiso, J. C., J. Yang, S. Honjo, and R. A. Krishfield (2003), Detection of change in the Arctic using satellite and in situ data, *J. Geophys. Res.*, *108*(C12), 3384, doi:10.1029/2002JC001347.

Davis, C., and A. Ferguson (2004), Elevation change of the Antarctic ice sheet, 1995–2000, from ERS-2 satellite radar altimetry, *IEEE Trans. Geosci. Remote Sens.*, *42*, 2437–2445.

Davis, C. H., C. A. Kluever, and B. J. Haines (1998), Elevation change of the southern Greenland ice sheet, *Science*, *279*, 2086–2088.

Davis, C. H., C. A. Kluever, B. J. Haines, C. Perez, and Y. T. Yoon (2000), Improved elevation change measurement of the southern Greenland ice sheet from satellite radar altimetry, *IEEE Trans. Geosci. Remote Sens.*, *38*, 1367–1378.

Early, D. S., and D. G. Long (2001), Image reconstruction and enhanced resolution imaging from irregular samples, *IEEE Trans. Geosci. Remote Sens.*, *39*, 291–302.

Fahnestock, M., R. Bindschadler, R. Kwok, and H. Jezek (1993), Greenland ice sheet surface properties and ice dynamics from ERS-1 SAR imagery, *Science*, *262*, 1530–1534.

Hall, D. K., R. S. Williams Jr., K. A. Casey, N. E. DiGirolamo, and Z. Wan (2006), Satellite-derived, melt-season surface temperature of the Greenland ice sheet (2000–2005) and its relationship to mass balance, *Geophys. Res. Lett.*, *33*, L11501, doi:10.1029/2006GL026444.

Hicks, B. R. and D. G. Long (2005), Improving temporal resolution of SIR images for QuikSCAT in the polar regions, report, Brigham Young Univ., Provo, Utah.

Jezek, K. C., P. Gogineni, and M. Shanableh (1994), Radar measurements of melt zones on the Greenland ice sheet, *Geophys. Res. Lett.*, *21*, 33–36.

Kalnay, E., et al. (1996), The NCEP/NCAR 40-year reanalysis project, *Bull. Am. Meteorol. Soc.*, *77*, 437–471.

Koerner, R. M. (1979), Accumulation, ablation and oxygen isotope variations in the Queen Elizabeth Island ice caps, Canada, *J. Glaciol.*, *22*, 25–41.

Krabill, W., et al. (2004), Greenland ice sheet: Increased coastal thinning, *Geophys. Res. Lett.*, *31*, L24402, doi:10.1029/2004GL021533.

Long, D. G., and M. R. Drinkwater (1994), Greenland ice-sheet surface properties observed by the Seasat-A scatterometer at enhanced resolution, *J. Glaciol.*, *40*, 213–230.

Long, D. G., and M. R. Drinkwater (1999), Cryosphere applications of NSCAT data, *IEEE Trans. Geosci. Remote Sens.*, *37*, 1671–1684.

Long, D. G. and B. R. Hicks (2005), Standard BYU QuikSCAT/SeaWinds land/ice image products, report, Brigham Young Univ., Provo, Utah.

Long, D. G., P. J. Hardin, and P. T. Whiting (1993), Resolution enhancement of spaceborne scatterometer data, *IEEE Trans. Geosci. Remote Sens.*, *32*, 700–715.

McConnell, J. R., R. J. Arthern, E. Mosley-Thompson, C. H. Davis, R. C. Bales, R. Thomas, J. F. Burkhart, and J. D. Kyne (2000), Changes in

Greenland ice sheet elevation attributed primarily to snow accumulation variability, *Nature*, *406*, 877–879.

Mote, T. L. (1998a), Mid-tropospheric circulation and surface melt on the Greenland ice sheet, part I, Atmospheric teleconnections, *Int. J. Climatol.*, *18*, 111–130.

Mote, T. L. (1998b), Mid-tropospheric circulation and surface melt on the Greenland ice sheet, part II, Synoptic climatology, *Int. J. Climatol.*, *18*, 131–146.

Mote, T. L., and M. R. Anderson (1995), Variations in snowpack melt on the Greenland ice sheet based on passive-microwave measurements, *J. Glaciol.*, *41*, 51–60.

Nghiem, S. V., K. Steffen, R. Kwok, and W. Y. Tsai (2001), Detection of snowmelt regions on the Greenland ice sheet using diurnal backscatter change, *J. Glaciol.*, *47*, 539–547.

Nghiem, S. V., K. Steffen, G. Neumann, and R. Huff (2005), Mapping of ice layer extent and snow accumulation in the percolation zone of the Greenland ice sheet, *J. Geophys. Res.*, *110*, F02017, doi:10.1029/2004JF000234.

Ohmura, A., and N. Reeh (1991), New precipitation and accumulation maps for Greenland, *J. Glaciol.*, *37*, 140–148.

Putnins, P. (1970), The climate of Greenland, in *World Survey of Climatology*, vol. 14, *Climates of Polar Regions*, edited by S. Orvig, pp. 3–128, Elsevier, New York.

Scott, J. B. T., D. Mair, P. Nienow, V. Parry, and E. Morris (2006a), A ground-based radar backscatter investigation in the percolation zone of the Greenland ice sheet, *Remote Sens. Environ.*, *104*, 361–373.

Scott, J. B. T., P. Nienow, D. Mair, V. Parry, E. Morris, and D. J. Wingham (2006b), Importance of seasonal and annual layers in controlling backscatter to radar altimeters across the percolation zone of an ice sheet, *Geophys. Res. Lett.*, *33*, L24502, doi:10.1029/2006GL027974.

Spencer, M. W., C. Wu, and D. G. Long (2000), Improved resolution backscatter measurements with the SeaWinds pencil-beam scatterometer, *IEEE Trans. Geosci. Remote Sens.*, *38*, 89–104.

Steffen, K., and J. Box (2001), Surface climatology of the Greenland ice sheet: Greenland Climate Network 1995–1999, *J. Geophys. Res.*, *106*, 33,951–33,964.

Steffen, K., S. V. Nghiem, R. Huff, and G. Neumann (2004), The melt anomaly of 2002 on the Greenland ice sheet from active and passive microwave satellite observations, *Geophys. Res. Lett.*, *31*, L20402, doi:10.1029/2004GL020444.

Stroeve, J., and K. Steffen (1998), Variability of AVHRR-derived clear-sky surface temperature over the Greenland ice sheet, *J. Appl. Meteorol.*, *37*, 23–31.

Tedesco, M. (2007), Snowmelt detection over the Greenland ice sheet from SSM/I brightness temperature daily variations, *Geophys. Res. Lett.*, *34*, L02504, doi:10.1029/2006GL028466.

Thomas, R. H., E. Frederick, W. Krabill, S. Manizade, and C. Martin (2006), Progressive increase in ice loss from Greenland, *Geophys. Res. Lett.*, *33*, L10503, doi:10.1029/2006GL026075.

Tsai, W.-Y., S. V. Nghiem, J. N. Huddleston, M. W. Spencer, B. W. Stiles, and R. D. West (2000), Polarimetric scatterometry: A promising technique for improving ocean surface wind measurements, *IEEE Trans. Geosci. Remote Sens.*, *38*, 1903–1921.

Ulaby, F. T., and W. H. Stiles (1981), Microwave response of snow, *Adv. Space Res.*, *1*(10), 131–149.

Wang, L., M. J. Sharp, B. Rivard, S. Marshall, and D. Burgess (2005), Melt season duration on Canadian Arctic ice caps, 2000–2004, *Geophys. Res. Lett.*, *32*, L19502, doi:10.1029/2005GL023962.

Williams, R. S., Jr., D. K. Hall, and C. S. Benson (1991), Analysis of glacier facies using satellite techniques, *J. Glaciol.*, *37*, 120–128.

Wismann, V. R. (2000), Monitoring of seasonal snowmelt in Greenland with ERS scatterometer data, *IEEE Trans. Geosci. Remote Sens.*, *38*, 1821–1826.

Zwally, H. J., and J. Li (2002), Seasonal and interannual variations of firn densification and ice sheet surface elevation at the Greenland summit, *J. Glaciol.*, *48*, 199–207.

Zwally, H. J., A. C. Brenner, J. A. Major, R. A. Bindschadler, and J. G. Marsh (1989), Growth of Greenland ice sheet: Measurement, *Science*, *246*, 1587–1589.

Zwally, H. J., M. B. Giovinetto, J. Li, H. G. Cornejo, M. A. Beckley, A. C. Brenner, J. L. Saba, and D. Yi (2005), Mass changes of the Greenland and Antarctic ice sheets and shelves and contributions to sea-level rise: 1992–2002, *J. Glaciol.*, *51*, 509–527.

B. Rivard and M. Sharp, Department of Earth and Atmospheric Sciences, University of Alberta, Edmonton, AB, Canada T6G 2E3.

K. Steffen, Cooperative Institute for Research in Environmental Sciences, University of Colorado, Boulder, CO 80302, USA.

L. Wang, Climate Research Division, Atmospheric Science and Technology Directorate, Environment Canada, 4909 Dufferin Street, Toronto, ON, Canada M3H 5T4. (libo.wang@ec.gc.ca)